CONF-860441--1

DE86 011507

EVENT SIMULATION FOR THE WA80 EXPERIMENT*

Soren P. SORENSEN

University of Tennessee, Knoxville, TN 39996, U.S.A., and
Oak Ridge National Laboratory, Oak Ridge, TN 37831, U.S.A.

The HIJET and LUND event generators are compared. It is concluded that for detector construction and design of experimental setups, the differences between the two models are marginal. The coverage of the WA80 setup in pseudorapidity and energy is demonstrated. The performance of some of the WA80 detectors (zero-degree calorimeter, wall calorimeter, multiplicity array, and SAPHIR lead-glass detector) is evaluated based on calculations with the LUND or the HIJET codes combined with codes simulating the detector responses.

1. INTRODUCTION

It is a common misconception among physicists that simulations are only a substitute for the real experimental data. This is not necessarily the case. Many aspects of a complicated experimental setup can often be studied only by doing simulation calculations: trigger bias, resolution of complicated experimental quantities, distortion effects from limited detector coverage, off-line data analysis algorithms, etc. For the ultrarelativistic heavy-ion program, we are, furthermore, faced with the situat'on that the experimental conditions, to a large extent, are unknown, and we have to rely on event generators in order to get a feeling for what to expect at the SPS in CERN or the AGS in Brookhaven..

In the WA80 collaboration, simulations have been used extensively for studying many aspects of our setup. In the following, some examples will be given to illustrate this.

2. LUND VS. HIJET

At the time the WA80 event simulations were started, there existed two different event generators, HIJET[1] and the LUND model.[2] A natural first step was to compare these two models in order to evaluate to what extent the final results of any simulation calculation will depend on the choice of event generator. The physics behind the event generators will not be discussed here since this is covered in a special section of these proceedings.

*Research sponsored by the U.S. Department of Energy under contract DE-AS05-76ER04936 with the University of Tennessee and under contract DE-AC05-840R21400 with Martin Marietta Energy Systems, Inc.

In fig. 1 are shown contour plots of the kinetic energy per particle versus the pseudorapidity obtained from both LUND and HIJET. Note that the HIJET calculation is done at a slightly lower beam momentum of 200A GeV/c, as compared to 225A GeV/c for the LUND calculation. Only central events with total particle multiplicities larger than 500 have been included. This type of plot is very useful in the design of the experimental setup since the typical energies and the energy ranges for which the detectors at the different angles should be sensitive can be read directly. The forward-angle detectors should be able to detect particles with energies ranging from 1 up to 200 GeV. Detectors in the mid-rapidity region should be sensitive from 100 MeV up to 10 GeV, and finally, detectors at 90° should be sensitive in the range from 10 MeV to 1 GeV.

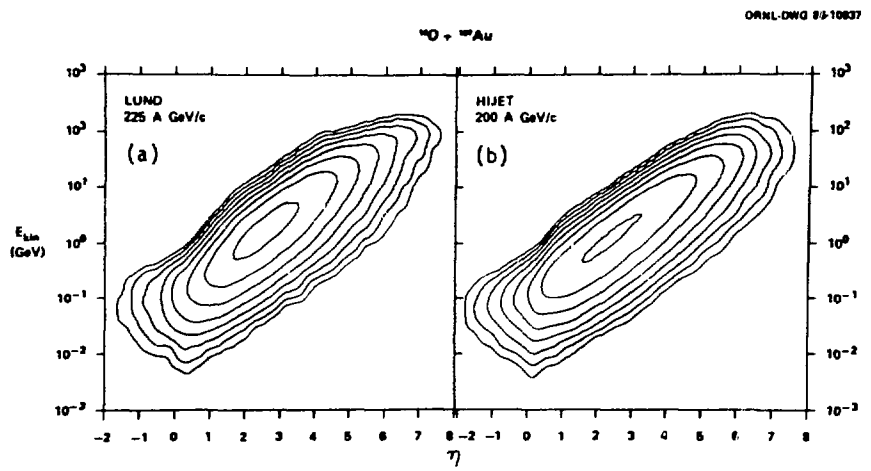

FIGURE 1
Contour plots of the kinetic energy versus pseudorapidity of each particle emitted by the event generator codes LUND and HIJET. Only central events with multiplicities larger than 500 have been selected. The outer contour line corresponds to 1 particle/(energy decade)/(unit in η). The contour lines closer to the maximum then correspond to densities of 2, 4, 8, etc.

By comparing figs. 1a and 1b, it is seen that the predictions of the two event generators are very similar and that most of the small differences are caused by the slightly lower beam energy in the HIJET case. Different event selections can be defined: (a) minimum bias, where all events generated by the codes are included; (b) peripheral, where only events with multiplicities lower than, e.g., 100 are selected; (c) charged particles, where only the charged particles within each event are studied; (d) π^0, where only the photons coming from π^0 decay are selected, etc. For all these cases the LUND and HIJET models give very similar predictions when plotted in an E_{kin} vs. η plane.

If quantities less dependent on the kinematics are compared, then some differences begin to turn up. This is illustrated in fig. 2, where the transverse energy spectra from the two models are compared, based on 1000 minimum bias events. HIJET gives a slightly larger average $E_\perp$; whereas, the LUND model, which in general seems to predict larger fluctuations, predicts a larger maximal value of $E_\perp$.

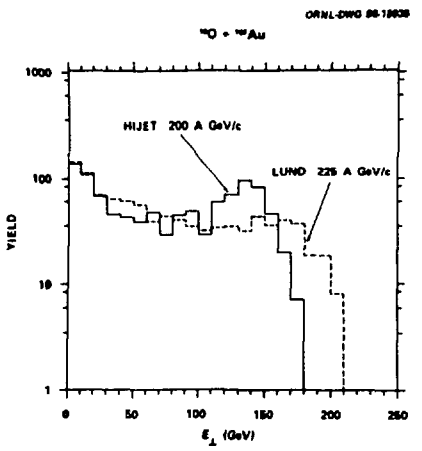

FIGURE 2
$E_\perp$ spectra from LUND and HIJET with minimum bias trigger. Based on 1000 events.

It can be concluded that, as long as the two models are used for simulations of detector performance and design of experimental configurations, they are essentially equivalent and that the differences between them probably are smaller than the absolute uncertainty by which they simulate the reality.

3. EVENT COVERAGE

The WA80 collaboration is putting much emphasis on performing a survey of the global characteristics of the ultrarelativistic heavy-ion collisions. In order to do this, it is important to have as large a coverage as possible of each event, not only in pseudorapidity but also in energy. This is demonstrated in fig. 3, which shows the same contour plot as in fig. 1a, but here the coverage of some of the detector elements of the WA80 setup has been indicated by shaded areas. (For a detailed discussion of the different WA80 detectors, see ref. 3.) A very high percentage (up to 80%) of all generated particles will be registered by the energy-sensitive detectors. The plastic ball seems to be very well suited for the pseudorapidity interval where it is placed; whereas, a metal scintillator sampling calorimeter, such as the wall,

will be of much more limited use at these large angles, due to its much worse energy resolution below 1 GeV and coarser angular granularity. From the plastic ball's performance at the Bevalac, it is also known that it is well suited for measuring the target spectator fragments, which are not generated by either the LUND model or HIJET and therefore are not included in fig. 3.

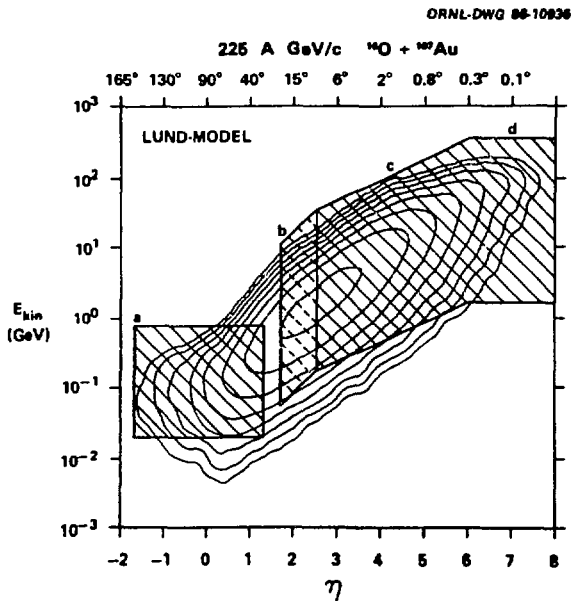

FIGURE 3
Kinetic energy and pseudorapidity coverage of the WA80 setup. The contour plot is identical to fig. 1a. The areas shaded with solid lines correspond to detectors with complete azimuthal coverage; whereas, the areas shaded with dashed lines correspond to only partial azimuthal coverage. (a) plastic ball, (b) SAPHIR and fifth box of the wall calorimeter, (c) the four quadrants of the wall, (d) the zero-degree calorimeter.

By varying the photomultiplier voltage on the wall calorimeter as a function of the distance to the beam line, the coverage of the wall can be adjusted to the shape of the typical event in the (E_{kin}, η) plane as indicated on area (c). This feature makes a calorimeter a very versatile instrument.

4. THE ZERO-DEGREE CALORIMETER

The purpose of the zero-degree calorimeter (ZDC) is to measure the total kinetic energy of the projectile fragments in order to use this as a trigger signal. Monte Carlo calculations by T. Gabriel (ORNL) with the high-energy

transport code HETC were performed in the design phase of the ZDC in order to ensure maximal energy resolution. At 50A GeV/c the relative energy resolution for ^{16}O will be 6%.

The ideal minimum bias trigger would allow the triggering on events where only one nucleon in the projectile has interacted with the target. This is not quite possible, since with a target of 0.5% interaction lengths, the frequency of a non-interacting mass-16 projectile will be at least a factor of 1000 larger than any projectile fragment with mass lower than 16. Based on the LUND model predictions for the projectile fragment mass distributions and the HETC calculated energy resolutions, it is estimated that at 50A GeV/c a loss of three nucleons by the projectile can be clearly distinguished; whereas at 200 GeV/c this will improve to two nucleons.

A central event is characterized by the absence of any projectile fragments. The perfect central trigger would then be the absence of any energy deposited in the ZDC. LUND model calculations, combined with GEANT geometry simulations, have shown that this cannot be completely obtained, since a number of the leading particles will come out of the reaction at such small angles that they pass along the beam pipe and dump their energy in the ZDC. A realistic central trigger will, therefore, not have its threshold set at the lowest possible energy, but more typically at an energy of 1-2 times the beam energy per nucleon.

5. WALL CALORIMETER

The wall calorimeter is one of the primary WA80 detectors, and many aspects of its performance have been simulated. Since the use of Monte Carlo codes such as HETC is extremely CPU-time consuming, we have chosen to use an analytical parameterization of the energy deposition of electromagnetic and hadronic showers very similar to the one used by the UA1 group.[4] The parameters for this parametrization were chosen by least square fits to HETC results. Also, the light collection in the sampling calorimeter is simulated by taking the attenuation in both the scintillator and the wavelength shifter into account. Due to the stochastic nature of a shower, the energy deposited in the calorimeter will have large fluctuations, both in total magnitude and spatial position. These fluctuations have been approximated by randomly varying the origin of the shower, the total deposited energy, and the length and radial size of the shower. The magnitude and probability distributions for these variations were determined from HETC calculations. Further fluctuations were introduced by depositing the energy in approximately 100 points selected according to the geometrical shape of the shower.

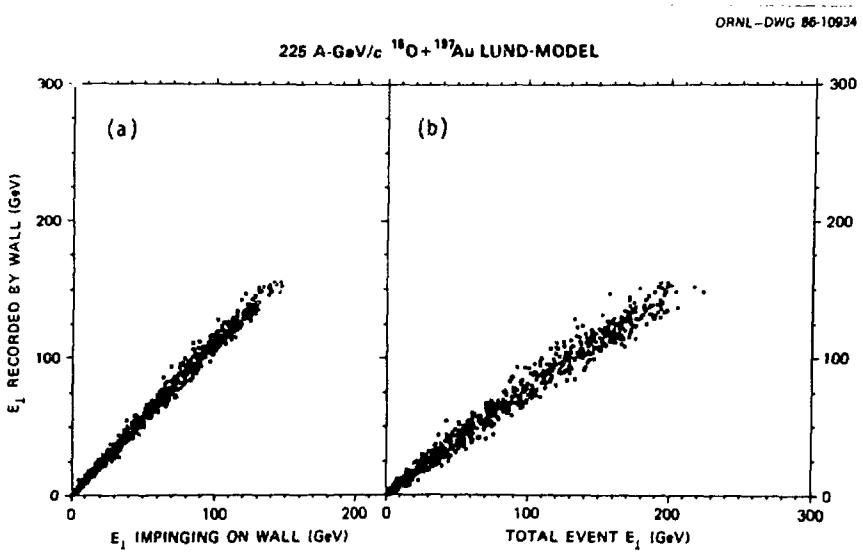

FIGURE 4
(a) Correlation between total transverse energy impinging on the wall calorimeter and the transverse energy recorded by the wall after the detector resolution has been taken into account. (b) Correlation between the total transverse energy in an event and the transverse energy recorded in the wall.

TABLE 1. $E_\perp$ resolution of wall calorimeter
(225A GeV/c ^{16}O + ^{197}Au, 1000 LUND events)

$E_\perp$ (GeV)	Total $E_\perp$ %	Hadronic $E_\perp$ %	"Electromagnetic" $E_\perp$ %
0-45	21	26	40
45-90	7	10	19
90-135	5.6	8.1	13
135-180	3.9	5.8	11
>180	3.5	5.5	10

The numbers shown are the second moment of the distributions for the following three quantities, respectively:

Column 2: $E_\perp$ recorded by wall / $E_\perp$ incident on wall

Column 3: $E_\perp$ recorded by HA-section / hadronic $E_\perp$ incident on wall

Column 4: $E_\perp$ recorded by EM-section / "electromagnetic" $E_\perp$ incident on wall

Probably the most important quantity to be measured by the wall calorimeter is the transverse energy $E_\perp$. Figure 4a illustrates that this can indeed be done very accurately. The figure shows the strong correlation between the transverse energy impinging on the wall and the energy recorded by the wall. The resulting $E_\perp$ resolutions are shown in table 1. Note that at the highest transverse energies the $E_\perp$ resolution will be as good as 3.5%. However, if the total $E_\perp$ in an event has to be evaluated, larger uncertainties are introduced, as shown in fig. 4b. This is due to the fluctuations in both the number of leading particles going through the central 8×8 cm^2 hole in the wall and the number of particles being ejected at large angles. Preliminary simulation calculations indicate that, by exploiting the information from the plastic ball, the TOF fence, and the multiplicity array, these fluctuations can be reduced considerably.

Why is it possible to measure the impinging transverse energy with uncertainties of only a few percent when it is well-known that hadronic sampling calorimeters have typical resolutions of 40-50% for 1 GeV hadrons? The answer has to be found primarily in the very high particle multiplicities in the central events. In a typical central event for 200A GeV/c ^{16}O + ^{197}Au, 600-700 particles are created, out of which approximately 300 will hit the wall. Only particles that normally will initiate showers in the calorimeter are included in these numbers. The large particle multiplicities are further illustrated in fig. 5, which shows the particle multiplicity distribution

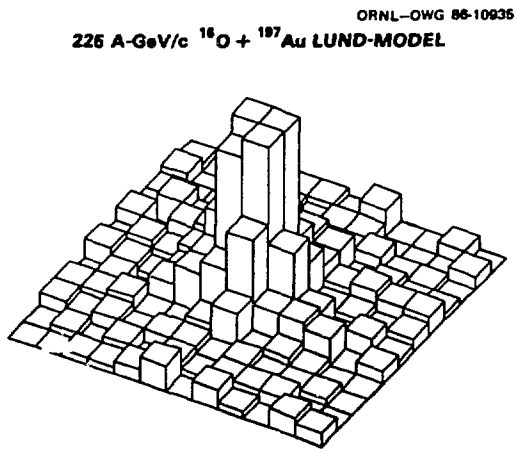

FIGURE 5
The multiplicity of particles hitting each tower of the wall calorimeter for a central event. The highest "skyscraper" corresponds to 21 particles.

across the face of the wall. Each LEGO-block corresponds to a 20 x 20 cm^2 tower. LUND simulations have shown that, for 1000 events, for 225A GeV/c $^{16}O + ^{197}Au$ run in the minimum bias trigger mode, up to 40 particles will hit a central tower, with the average at 16. At 5° the average has decreased to one, and the multiplicity distribution is converging towards a Poisson distribution. At the largest angles of 10°, the average multiplicity per tower is 0.3, with a double hit probability around 2%.

These high multiplicities emphasize that for ultrarelativistic heavy-ion reactions, calorimeters will have to be used in a different way than for hadron-induced reactions where the multiplicities are much smaller. In the latter experiments, hadronic calorimeters have very often been used to search for jet structures,[5] and typically the emphasis in the off-line analysis has been to identify one or more strong clusters of towers where a large amount of energy has been deposited. With the high multiplicities in the heavy-ion experiments, the emphasis will change to a more global analysis of the energy deposition.

It is, however, very important to realize that the high multiplicities in many ways will improve the performance of the calorimeters. Since each tower will be sampling many showers, the large fluctuations in the energy deposition will be reduced. This is a simple consequence of the Central Limit Theorem, which can be illustrated by comparing two situations: (a) one 100-GeV hadron or (b) ten 10-GeV hadrons impinging on a calorimeter. The energy resolution in the two cases will be the same ($40\%/\sqrt{100} = 4\%$), but the fluctuations in the origin and the length and radial size of the showers will be $\sqrt{10}$ smaller in case b. This implies that a much better separation of the electromagnetic and hadronic energy can be obtained. For 225A GeV $^{16}O + ^{197}Au$, simulations have shown that, on the average, 20% of the energy carried by hadrons is deposited in the EM section of the wall. Instead of using the raw energy deposited in the EM section, a better estimate of the energy carried by electrons and photons can be obtained by subtracting one-fourth of the energy deposited in the hadronic section from the raw energy deposited in the EM section. Such a correction would be very inaccurate in a low multiplicity situation, where the fluctuations in the origin of the hadronic showers would dominate, but for high multiplicities it provides a much improved estimate of the energy carried by hadronic and "electromagnetic" particles.

Arguments like this can be extended also to take into account the leaking of showers between towers. Based on simulation tests, an event restoration algorithm for the wall calorimeters has been developed. The algorithm is

essentially identical to the method used to unfold the detector response of the Spin Spectrometer at The Holifield Heavy Ion Facility in Oak Ridge.

Based on simulations, the response matrix $\underline{\underline{R}}$ of the calorimeter can be calculated. If the towers in the electromagnetic sections are labeled by odd integers (starting at 1) and the towers in the hadronic sections are labeled by even integers (starting at 2), then the matrix element R_{ji} of the response matrix can be defined as the fraction of the energy originally hitting element i which will show up in element j after the shower. If the incident particle is a hadron, then i will be an even number; otherwise, i is odd. Due to the large fluctuations from event to event, R_{ji} has to be calculated as the average over many events. Since different types of events, such as peripheral and central events, will have different energy distributions, then it is necessary to operate with different response functions for different classes of events. If the measured energy in the j'th element is b_j, then the energy x_i impinging on the element i can be estimated by solving the following set of linear equations:

$$b_j = \sum_i R_{ji}\, x_i$$

or in matrix form

$$\underline{b} = \underline{\underline{R}}\, \underline{x} \ .$$

The accuracy of this assumption depends on the magnitude of the fluctuations in the response of the detector. In a high multiplicity situation where the fluctuations are small, it is a reasonably good approximation. This linear system cannot be solved by just multiplying through with the inverse matrix of $\underline{\underline{R}}$, since in that case the small fluctuations (statistical noise) will be amplified by the inverse matrix and the final energy distribution will be strongly fluctuating. (For a more detailed discussion of this point, see ref. 6.) Instead, an iterative algorithm has to be used, and we have found the following method to be both fast and robust.[7]

Initial guess: $\underline{x}_0 = \underline{b}$

n'th iteration: $\underline{c}_n = \underline{b} - \underline{\underline{R}}\, \underline{x}_n$

$$\underline{x}_{n+1} = \underline{x}_n - \frac{\|\underline{c}_n\|^2}{\|\underline{\underline{R}}'\, \underline{c}_n\|^2}\, \underline{\underline{R}}'\, \underline{c}_n \ ,$$

where $\|\ \|$ denotes the Euclidean norm, and $\underline{\underline{R}}'$ is the transposed matrix of $\underline{\underline{R}}$. Better results can be obtained by using some of the many nonlinear algorithms developed for image restoration, such as the maximum entropy method,[8] but they are in general too slow.

An example of the use of the event restoration is shown in fig. 6. The upper row shows the incident hadron and EM energy and constitutes the distribution $\underline{x}$ which the event restoration algorithm is supposed to re-create. The middle row shows the simulated energy deposition of the same event in each tower and section corresponding to the distribution $\underline{B}$. Note how especially the EM section is distorted. Finally, the bottom row shows the energy distributions after application of the event restoration algorithm. Note especially how the details of the energy deposition in the central EM towers have improved.

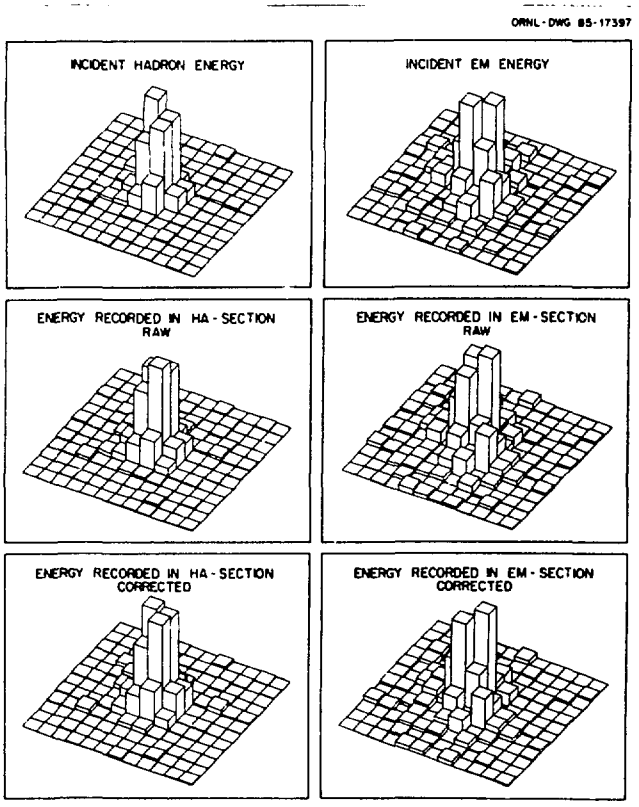

FIGURE 6

Demonstration of the wall calorimeter event restoration algorithm. The LEGO-plots show the energy in each tower of the hadronic and electromagnetic sections of the wall calorimeter for a single central event. The upper row shows the energy impinging on the face of the calorimeter; the middle row shows the energy deposited in each tower; and finally, the bottom row shows the energy distribution after the event restoration algorithm has been applied.

6. MULTIPLICITY ARRAY

The purpose of the multiplicity arrays will be to measure η distributions of charged particles ($dN/d\eta$) with a very small bin size in η of the order of 0.05. This extremely fine granularity should also allow a restricted form of speckle interferometry analysis of the data or an analysis of fluctuations in $dN/d\eta$ along the lines demonstrated by the UA5 collaboration.[9]

A major design criterion for the multiplicity arrays has been to use pad sizes small enough to avoid double hits. LUND model simulations have demonstrated that at 225A GeV/c ^{16}O + ^{197}Au, the double hit probability for each pad is always lower than 0.5%, and for most pads it is lower than 0.1%. The typical total number of double hits for a central event with a charged-particle multiplicity above 350 is 1-2.

7. THE SAPHIR LEAD-GLASS WALL

The main purposes of the SAPHIR detector system are to detect direct single photons from the quark-gluon phase and to measure the π^0 momentum distribution. In order to evaluate whether this is possible, HIJET simulations have been performed by the Munster group. All simulations for the SAPHIR detector presented here have been done for the reaction 50A GeV/c ^{16}O + ^{197}Au.

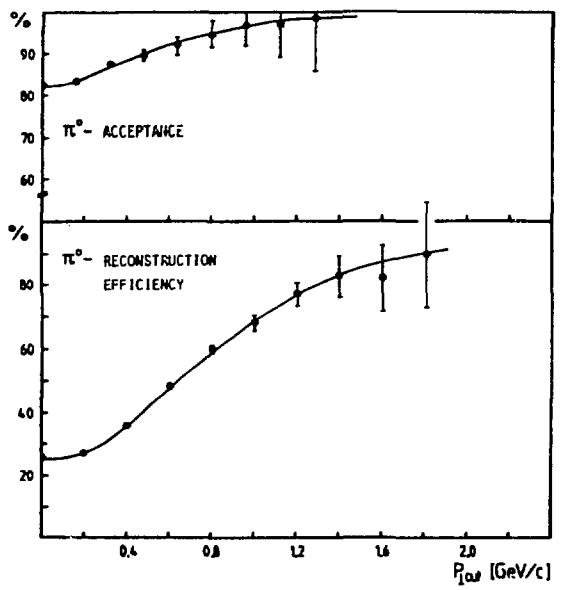

FIGURE 7
The efficiency for detecting and identifying π^0 in a single event. Refer to text for further details. The calculation is based on 54000 HIJET events for the reaction 50A GeV/c ^{16}O + ^{197}Au.

The quality of the π^0 detection on an event-by-event basis is demonstrated in fig. 7. For each event the invariant mass $M_{\gamma\gamma}$ of all possible photon pairs with transverse momenta larger than $P_{\perp cut}$ is calculated. A true π^0 is then identified as a photon pair with $M_{\gamma\gamma}$ in the interval between 127 and 143 MeV. Due both to the limited energy and angular resolution and the applied cut on $M_{\gamma\gamma}$, the acceptance of π^0's will always be below 100%. For $P_{\perp cut} > 1$ GeV, 90% of all π^0's originally headed towards the detector will be accepted by the reconstruction algorithm. This number ignores the loss in efficiency due to the unavoidable combinatorial problems. This is illustrated in fig. 7b, which

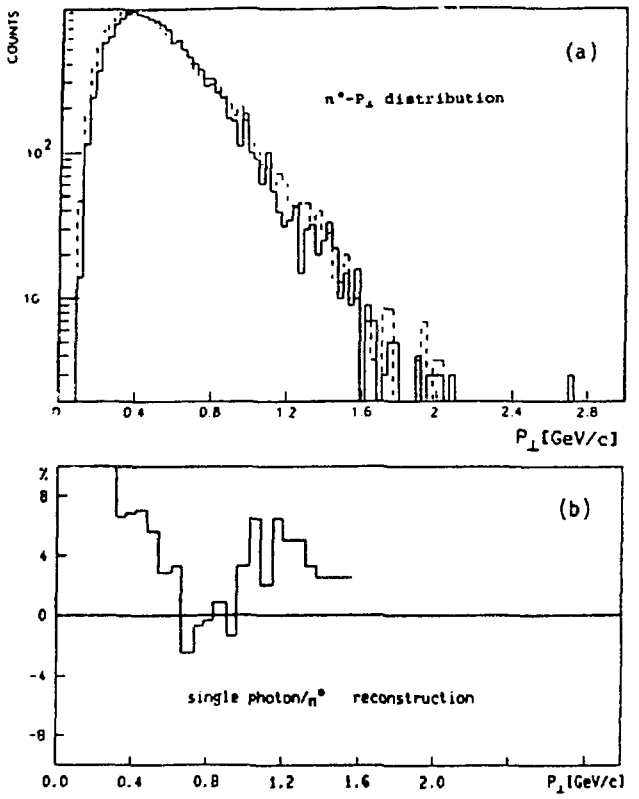

FIGURE 8
The upper part (a) shows, for the same calculation as in fig. 7, the $P_\perp$ distribution of π^0's as obtained by HIJET (solid line) and the reconstructed distribution (dashed line). The lower part (b) shows the reconstructed single photon to π^0 ratio, which for HIJET events is expected to be zero. Between 0.4 and 1.6 GeV/c, the average deviation is only 3%.

shows the π^0 reconstruction efficiency as function of $P_{\perp cut}$. For $P_{\perp cut} > 1.2$ GeV, the efficiency for detecting true π^0's in the proper mass region reaches 80%, which implies that, even in individual events, π^0's can be distinguished from single photons with 80% efficiency for sufficiently large $P_\perp$.

If, instead of an event-by-event analysis, a well-defined set of events is selected (corresponding to a given trigger or an off-line criterion), then a much better single photon detection efficiency can be obtained. By accumulating high statistics in the mass spectrum, the combinatorial background below the π^0 peak can be subtracted at the one percent level. In this way, very clean $P_\perp$ spectra and angular distributions for the π^0 can be obtained. Figure 8a shows the very good agreement between the reconstructed $P_\perp$ spectrum and the original HIJET spectrum.

Based on the reconstructed $P_\perp$ spectrum and the reconstructed π^0 angular distribution, the total number of photons in the detector originating from π^0's can be calculated. By comparing this number with the actual observed number of photons, the number of surplus photons can be determined. In the HIJET calculations this surplus is expected to be zero. The deviation from zero in derived surplus photons therefore tells us the uncertainty in the extraction of the surplus number. For $P_\perp$ larger than 0.8 GeV the average deviation is 3%, which implies that we should be able to detect single photons down to a level of at least 5% of the π^0's.

REFERENCES

1) T. Ludlam, this volume.

2) B. Anderson, this volume.

3) H. Gutbrod, this volume.

4) M. Della Negra, Phys. Scr. 23 (1981) 469.

5) O. Bottner, Ph.D. thesis, Niels Bohr Institute, Copenhagen, 1985.

6) R. L. Parker, Ann. Rev. Earth Planet. Sci. 5 (1977) 35.

7) N. Gastinel, Linear Numerical Analysis (Academic Press, Inc., New York, 1970), Sections 5.16 and 5.21.

8) B. R. Frieden, Jour. Opt. Soc. Amer. 62 (1972) 511 and S. F. Gull and G. J. Daniell, Nature 272 (1978) 686.

9) G. Ekspong, this volume.

DISCLAIMER